IEEE Access
Multidisciplinary | Rapid Review | Open Access Journal

Received October 3, 2018, accepted October 24, 2018, date of publication October 30, 2018, date of current version November 30, 2018.

Digital Object Identifier 10.1109/ACCESS.2018.2878623

High-Precision Anti-Disturbance Gimbal Servo Control for Control Moment Gyroscopes via an Extended Harmonic Disturbance Observer

LIYA HUANG, ZHONG WU, AND KAN WANG
School of Instrumentation Science and Optoelectronics Engineering, Beihang University, Beijing 100191, China
Corresponding author: Zhong Wu (wuzhong@buaa.edu.cn)

This work was supported by the National Natural Science Foundation of China under Grant 10772011.

ABSTRACT In control moment gyroscopes (CMGs), the gimbal is expected to rotate at a low speed with high precision so that high-precision gyroscopic torque can be generated to realize high-precision spacecraft attitude control. However, there are complex and multiple disturbances in the gimbal servo systems, which may deteriorate the gimbal control performance to a great extent. In this paper, an extended harmonic disturbance observer (EHDO)-based composite controller is proposed to reject the effects of multiple disturbances on the control performance of gimbal servo systems. Firstly, an EHDO is developed for an mth-order model describing disturbance dynamics in which the rotor dynamic imbalance torque along gimbal axis is modeled as a harmonic, and the others are approximated as a polynomial. Compared with conventional extended disturbance observers, EHDO can estimate multiple disturbances with high precision even with a lower bandwidth. Secondly, a backstepping-based composite controller is designed to achieve high-performance gimbal control for CMGs. Finally, simulation and experimental results are presented to demonstrate the effectiveness of the proposed method.

INDEX TERMS Anti-disturbance control, composite controller, control moment gyroscopes, extended harmonic disturbance observer, gimbal servo system.

NOMENCLATURE

m	order of disturbance model and observers
Ω	SGCMG rotor speed
ω	SGCMG gimbal speed
ω_d	desired gimbal speed
$\tilde{\omega}$	gimbal speed tracking error
u_d, u_q	stator voltages of d-axis, q-axis
i_d, i_q	stator currents of d-axis, q-axis
R	stator resistance
n_p	motor pole pairs
ψ_f	stator flux linkage
L_d, L_q	stator inductance of d-axis, q-axis
T_e	electromagnetic torque of PMSM
T_e^*	desired electromagnetic torque
$\tilde{T}_e$	electromagnetic torque tracking error
J	equivalent moment of inertia about the gimbal axis
D	damping coefficient about the gimbal axis
T_g	disturbance caused by gimbal system
T_r	disturbance caused by rotor rotation
T_s	disturbance caused by spacecraft motion
T_u	disturbance caused by unmodeled factors
u_r	the quantity of rotor dynamic imbalance
ϕ_d	initial phase of rotor dynamic torque
d	total disturbance in gimbal servo system
$\delta(t)$	the mth-order derivative of d in EDO or the $(m-2)$th-order derivative of $(d-T_r)$ in EHDO
l_j	observer gains, $j = a, b, 1, \ldots m$
λ	bandwidth of the EDO and EHDO
λ_p	maximal eigenvalue of $\boldsymbol{P}$
λ_q	minimal eigenvalue of $\boldsymbol{Q}$
δ_m	upper bound of $\delta(t)$
k_t	electromagnetic torque coefficient
k_0, k_1, k_2	controller gains

I. INTRODUCTION

As a kind of actuators for spacecraft attitude control, control moment gyros (CMGs) have been widely used in

fast maneuver of agile spacecraft and high-precision attitude stabilization of large spacecraft owing to their superior properties in simple structure, large torque and high precision [1]–[3]. A CMG typically consists of a high-speed rotor with large angular momentum and one or two low-speed gimbals [4]. By changing the direction of angular momentum via gimbal rotation, gyroscopic torque can be produced to control spacecraft attitude. It has been recognized that a crucial task of high precision control for spacecraft attitude control is to increase the accuracy of CMG torque which greatly depends on the control precision of gimbal servo systems.

However, there are various disturbances in gimbal servo systems, such as frictions, cogging effects, flux distortions, current ripples, and the disturbance caused by the rotor dynamic imbalance, spacecraft motions [5]–[7], etc. Although these disturbances have different features, all of them can degrade the control performance of gimbal servo systems significantly. Some of them are related to the gimbal motion such as frictions, cogging effects, and flux distortions, while some of them are related to the rotor rotation, such as rotor imbalance torque [8]–[10]. Since the gimbal moves at a low speed and the rotor rotates at a high speed, there is a great difference in the frequency of disturbances in the gimbal servo systems. It is such a wide range of disturbance frequency which brings great difficulties in disturbance attenuation and rejection for gimbal servo systems.

To overcome the adverse effects of disturbances, many disturbance attenuation strategies have been proposed, such as robust control [11]–[13], sliding mode control (SMC) [14]–[16], internal model principle (IMP) based control [17]–[21], etc. Although these control methods demonstrate strong robustness to disturbances and uncertainties, there still exist some deficiencies in them, such as the conservation of robust control, the chattering problem of SMC, and the strong dependence of disturbance model of IMP.

To avoid problems of the above methods, disturbance uncertainty estimation and attenuation (DUEA) techniques [22], [23] have been paid considerable attentions during the past several decades. The basic idea of DUEA is to estimate the disturbances and uncertainties with a disturbance estimator, and then compensate them effectively with the estimated value via feedforward. Furthermore, a feedback controller is applied to achieve desired control performance for closed-loop system. As an important component of DUEA, the performance of disturbance estimator affects the ability of disturbance attenuation and rejection to a great extent.

Up to now, various disturbance estimators have been proposed, such as disturbance observer (DO) [24]–[26], extended state observer (ESO) [5], [27]–[29], proportional integral observer (PIO) [30], etc. Both ESO and PIO estimate the lumped disturbance together with the system states, while DO only output the estimate of the lumped disturbance. As a reduced-order disturbance observer, DO is enough for gimbal servo systems since the gimbal angular position and speed are directly derived from resolver-to-digital converters.

In conventional DOs, all the uncertainties and disturbances are usually treated as derivative-bounded lumped disturbance [20], [31], thus the detailed model information of disturbances and uncertainties is no longer required during observer design. However, the assumption of bounded derivative for lumped disturbance may result in large model errors for high-order disturbances, which may lead to greater estimate error for DOs with limited bandwidth.

To attenuate the effects of disturbance model uncertainties on the estimation accuracy of high-order disturbances, sliding mode disturbance observer (SMDO) [32]–[36] is proposed by introducing sliding mode technology into disturbance observer design. Most of SMDOs are full order observers which give estimates for the lumped disturbance and the system states. For gimbal servo systems, additional estimation of system states may increase implementation cost [32]. Although reduced-order SMDO will not estimate system states repeatedly, the derivative of angular speed for spacecraft is approximated by using a tracking differentiator which also can increase the complexity of the observer [32]. In addition, the chattering phenomenon is still a severe problem to be solved for all SMDOs.

To avoid the problems of SMDO and improve estimation accuracy for high-order disturbances, extended disturbance observer (EDO) is proposed by describing the disturbance with a high-order model [3], [37], [38]. In EDO, the bandwidth should be chosen much greater than the frequency content of the estimated disturbances. However, larger observer bandwidth increases the sensitivity to noises [39]. As a type of high gain observers, EDO also leads to high gain problems for high-order disturbances.

To avoid the high gain problem of EDO and the chattering problem of SMDO, Chen proposed a harmonic disturbance observer (HDO) to estimate harmonic disturbance [40]. The harmonic disturbance is supposed to have known frequency but unknown amplitude and phase, and can be represented by a second-order neutral system. According to the second-order system describing harmonic disturbance, nonlinear harmonic observer including stability analysis and gain tuning approach is established for nonlinear systems with harmonic disturbances [40], [41]. Obviously, the order of HDO is the double of the number of harmonics in disturbances. As for gimbal servo systems in CMGs, there are multiple harmonics in disturbances which may lead to high order of HDO. Besides, HDO only focuses on dealing with harmonic disturbances and other aperiodic disturbances are not taken into account.

In order to improve the disturbance rejection ability for gimbal servo systems, an extended harmonic disturbance observer (EHDO) is designed to estimate the lumped disturbance described by an mth-order ($m \geq 3$) dynamical system. In this system, only the dynamic imbalance disturbance with the same frequency as the rotor is represented by a second-order harmonic model. The other ones are supposed to be slowly-varying and represented by a (m-2)th-order polynomial model. Hence, the lumped disturbance can be estimated precisely by using EHDO even with a lower bandwidth and

the high gain problem of EDO can be avoided. Thereafter, feedforward is used to compensate multiple disturbances in gimbal servo systems by using estimated disturbance from EHDO, and a backstepping based composite controller is designed to achieve expected control performance in gimbal speed control for CMGs.

The rest of the paper is organized as follows. In Section 2, the control problem of gimbal servo systems in CMGs is formulated after a brief introduction for mathematical models of gimbal dynamics and multiple disturbances is given. In Section 3, a conventional EDO is designed for gimbal servo systems and the problem of high gain is analyzed. Then, EHDO is proposed to estimate multiple disturbances in gimbal servo systems in Section 4 and the relationship between the estimation accuracy of disturbances and the observer parameters (including bandwidth and order) is also discussed. In Section 5, a composite controller is designed for gimbal servo systems via backstepping method. In Section 6, simulation results are given to show the effectiveness of the proposed method. Conclusions are made in Section 7.

II. MATHEMATICAL MODEL AND PROBLEM FORMULATION

As shown in Fig. 1, single gimbal CMG (SGCMG) is considered in this paper. In this section, the mathematical model of gimbal dynamics and multiple disturbances will be introduced first, and then the control problem of gimbal servo systems in CMGs will be formulated.

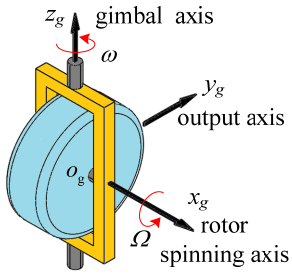

FIGURE 1. Single gimbal CMG.

A. DYNAMICS OF GIMBAL SERVO SYSTEM

For SGCMG, the rotor usually rotates about the spinning axis x_g at a constant and high speed Ω. When the gimbal rotates about the gimbal axis z_g at a low speed ω, gyroscopic torque will be generated along the output axis y_g owing to the variations of the rotor momentum in SGCMG.

In order to drive the gimbal rotating slowly and precisely, permanent magnet synchronous motor (PMSM) is often adopted in most of SGCMGs owing to its superior performance at low speed. Assuming that PMSM has a surface-mounted permanent magnet rotor, 3-phase wye-connected symmetric stator windings, and ideal back EMF of sinusoidal waveform, then the equations of voltage and current in d-q reference coordinates can be described by [23]

$$\begin{cases} u_d = L_d p i_d + R i_d - n_p \omega L_d i_q \\ u_q = L_q p i_q + R i_q + n_p \omega L_q i_d + n_p \omega \psi_f \end{cases} \tag{1}$$

where p is the differential operator.

Without consideration of salient and slot effects, magnetic saturation, and losses due to hysteresis and eddy current, the electromagnetic torque T_e of PMSM can be written as [23]

$$T_e = 1.5 n_p \left[\psi_f i_q + \left(L_d - L_q \right) i_d i_q \right] \tag{2}$$

Actuated by the electromagnetic torque T_e, the gimbal will rotate about the gimbal axis and the equation of motion can be given by [42]

$$J\dot{\omega} + D\omega = T_e - T_g - T_r - T_s - T_u \tag{3}$$

B. ANALYSIS OF THE MULTIPLE DISTURBANCES

For multiple disturbances of (3) in gimbal servo systems driven by PMSM, the characteristics will be analyzed.

1) DISTURBANCE RELATED TO GIMBAL SYSTEM

In (3), T_g represents the disturbances caused by unexpected factors in gimbal servo systems, such as motor-related factors including cogging effect and flux distortion [43], [44], control-related factors including current measurement error and PWM dead time effect, and bearing friction. Both motor-related and control-related factors may lead to ripple torques described by harmonic models in [45]. Since the ripple torques are very small in amplitude, only basic components of ripple torques are considered in this paper. For bearing frictions, Stribeck model is widely used to describe nonlinear effect of friction at low velocity [46]. Thus, T_g can be approximately expressed as

$$\begin{aligned} T_g = {} & T_{cog} \sin(N_{co}\theta) + T_{flux} \cos(6\theta_e) + T_d \cos(6\theta_e) \\ & + T_m \cos\theta_e + T_c \cdot sign(\omega) + (T_{st} - T_c) e^{-(\omega/\omega_s)^2} sign(\omega) \end{aligned} \tag{4}$$

where T_{cog}, T_{flux}, T_d and T_m are the amplitudes of basic components of ripple torques caused by cogging effect, flux harmonic, dead time effect and current measurement error, respectively; T_c and T_{st} are Coulomb and static friction torques respectively; N_{co} is the least common multiple between motor slots and poles; θ and θ_e denote mechanical and electrical angles respectively; ω_s is the Stribeck characteristic angular speed; sign$(\cdot)$ is a signum function with respect to $(\cdot)$.

From (4), it is obvious that ripple torques are periodic functions with angular frequencies related to gimbal speed and friction torques are signum function of gimbal speed. Since the gimbal often works at low speed in SGCMGs, the disturbances in (4) vary very slowly.

2) DISTURBANCE RELATED TO ROTOR DYNAMIC IMBALANCE

In (3), T_r represents the disturbance caused by dynamic mass imbalance of the rotor in SGCMGs. Dynamic imbalance

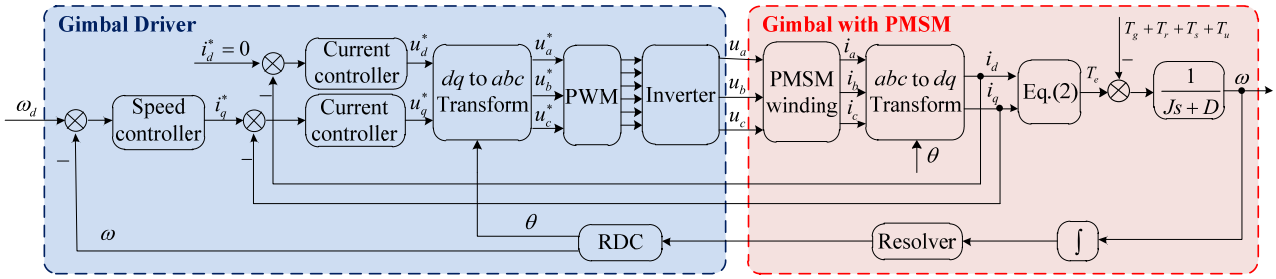

FIGURE 2. Schematic diagram of gimbal servo system.

arises when the principal axis of inertia does not coincide with the spinning axis of the rotor. When the rotor rotates at the velocity of Ω, dynamic imbalance will lead to a vector of radial centrifugal torque rotating in the perpendicular plane of the spinning axis [7]. Denoting the quantity of the rotor dynamic mass imbalance by u_r, then the rotor dynamic imbalance torque can be expressed along gimbal axis as follows [47]:

$$T_r = u_r \Omega^2 \sin(\Omega t + \phi_d) \tag{5}$$

From (5), it is known that the disturbance torque due to rotor dynamic imbalance has the amplitude proportional to Ω^2 and the same frequency as Ω. Since the rotor speed Ω is often very high to achieve large gyroscopic effect for SGCMG, the amplitude and frequency of T_r are much higher than the other disturbances in gimbal servo systems.

3) DISTURBANCE RELATED TO SPACECRAFT MOTION

In (3), T_s represents the disturbance caused by the angular motion of spacecraft. Let ω_{by} denote the component along the output axis y_g of the angular velocity of spacecraft, then the disturbance torque T_s can be expressed as [48]

$$T_s = -\omega_{by} I_r \Omega \tag{6}$$

where I_r denotes the inertia of the rotor.

From (6), it is known that the disturbance T_s is proportional to the angular velocity ω_{by} since the angular momentum $I_r\Omega$ is fixed for SGCMGs. When the spacecraft maneuvers rapidly, the amplitude of T_s will be very large. Considering the practical mode of attitude maneuver for spacecraft, T_s can be approximated to be a polynomial model.

C. PROBLEM FORMULATION

Multiple disturbances in gimbal servo systems may bring great difficulties in high-precision gimbal control for CMGs. In this paper, a cascade control structure is adopted to attenuate the effects of multiple disturbances on gimbal control performance for SGCMGs, as shown in Fig. 2. Then, the control problem of gimbal servo system for SGCMGs can be formulated as follows.

For the gimbal servo system (1)-(3), the objective of this paper is given as follows. 1) Design a disturbance observer to estimate the lumped disturbance in (3) with high precision and the estimate error can be confined in a bounded region which can be regulated by the observer gains. 2) Design a composite controller to track the desired gimbal speed with high precision by using feedforward compensation and feedback regulation, and the tracking error can be confined in a bounded region which can be regulated by the controller gains.

III. DESIGN AND ANALYSIS OF CONVENTIONAL EDO

In this section, the lumped disturbance in (3) is modeled as an mth-order ($m \geq 3$) polynomial first. Then, a conventional EDO is designed for the mth-order disturbance model and the observer performance is analyzed.

A. POLYNOMIAL BASED DISTURBANCE MODEL

Denoting the lumped disturbance in (3) by d, then we can get $d = T_g + T_r + T_s + T_u$. According to (3), the lumped disturbance d also can be expressed as

$$d = T_e - J\dot{\omega} - D\omega \tag{7}$$

Theoretically, the lumped disturbance d can be obtained from (7) if both angular velocity ω and electromagnetic torque T_e are available. In engineering, it is not feasible to obtain d by using (7) since the calculation of the angular acceleration $\dot{\omega}$ will amplify higher-frequency noise components in ω. Therefore, disturbance observer is a feasible way to obtain the estimate of the lumped disturbance.

In order to design an observer to estimate the lumped disturbance, its model should be established first. In the theory of numerical approximations, a common function is polynomial. Similarly, the lumped disturbance d can be approximated by using an mth-order polynomial as $d = \alpha_0 + \alpha_1 t + \alpha_2 t^2 + \cdots + \alpha_m t^m$ with coefficients αi, $i = 0, 1, \cdots, m$. By defining the states $x_1 = d$, $x_2 = \dot{d}$, $\cdots$, $x_m = d^{(m-1)}$, the polynomial model also can be expressed by an mth-order dynamical system as

$$\begin{cases} \dot{x}_j = x_{j+1}, & j = 1, 2, \cdots, m-1 \\ \dot{x}_m = d^{(m)} \end{cases} \tag{8}$$

Regard d derived from (7) as a virtual measurement of the lumped disturbance, then the virtual output equation of (8) can be written as

$$d = x_1 \tag{9}$$

Thus, the mth-order dynamical system describing the dynamics of the lumped disturbance is established.

B. DESIGN OF EDO

Let $\hat{x}_j$ and $\hat{d}$ represent the estimate of x_j and the prediction of d respectively, $j = 1, \cdots, m$, then a state observer for (8) and (9) can be designed as

$$\begin{cases} \dot{\hat{x}}_j = \hat{x}_{j+1} + l_j(d - \hat{d}), \ j = 1, 2, \cdots, m-1 \\ \dot{\hat{x}}_m = l_m(d - \hat{d}) \end{cases} \tag{10}$$

where $\hat{d} = \hat{x}_1$; l_j are observer gains, $j = 1, \cdots, m$.

Substituting (7) and (9) into (10) gives

$$\begin{cases} \dot{\hat{x}}_j = \hat{x}_{j+1} + l_j(T_e - J\dot{\omega} - D\omega - \hat{x}_1), \ j = 1, 2, \cdots, m-1 \\ \dot{\hat{x}}_m = l_m(T_e - J\dot{\omega} - D\omega - \hat{x}_1) \end{cases} \tag{11}$$

In order to avoid the calculation of the angular acceleration $\dot{\omega}$, auxiliary variables z_j are introduced to satisfy

$$\hat{x}_j = z_j - l_j J\omega, \quad j = 1, 2, \cdots, m \tag{12}$$

According to (12), (11) can be rewritten as

$$\begin{cases} \dot{z}_j = z_{j+1} - l_{j+1}J\omega + l_j(T_e - D\omega - z_1 + l_1 J\omega) \\ \dot{z}_m = l_m(T_e - D\omega - z_1 + l_1 J\omega), \quad j = 1, 2, \cdots, m-1 \end{cases} \tag{13}$$

Thus, (12) and (13) constitute an extended disturbance observer to estimate multiple disturbances in (3) [3].

C. ANALYSIS OF EDO

In order to analyze the performance of the conventional EDO, the error dynamics of the conventional EDO should be obtained first. Since EDO in (12) and (13) is obtained by the variable substitutions of (10), the error dynamics for (10) can be examined instead.

Define the estimate errors as $\tilde{x}_j = x_j - \hat{x}_j, j = 1, \cdots, m$ and $\tilde{d} = d - \hat{d}$, then the error dynamics of EDO can be derived from (9) and (10) as follows:

$$\begin{cases} \dot{\tilde{x}}_j = \tilde{x}_{j+1} - l_j\tilde{d}, \quad j = 1, 2, \cdots, m-1 \\ \dot{\tilde{x}}_m = d^{(m)} - l_m\tilde{d} \end{cases} \tag{14}$$

According to (14), the transfer function from the lumped disturbance d to the estimate error $\tilde{d}$ can be obtained as

$$G_1(s) = \frac{\tilde{d}(s)}{d(s)} = \frac{s^m}{s^m + l_1 s^{m-1} + l_2 s^{m-2} + \cdots l_m} \tag{15}$$

If the observer gains are chosen as

$$l_j = \frac{m!}{j!\,(m-j)!}\lambda^j, \quad j = 1, 2, \cdots, m \tag{16}$$

Then (15) will have multiple poles at $s = -\lambda$ which also determines the bandwidth of EDO [49].

To demonstrate the performance of EDO with different bandwidths and orders, the frequency characteristics of $G_1(s)$ can be plotted. Fig. 3 shows the frequency response of $G_1(s)$ for the 3rd-order EDO with different bandwidths ($\lambda = 2\pi$, 10π, 50π rad/s). Fig. 4 shows the frequency response of $G_1(s)$ for the EDO with fixed bandwidth ($\lambda = 2\pi$ rad/s) and different orders ($m = 3, 4, 5$).

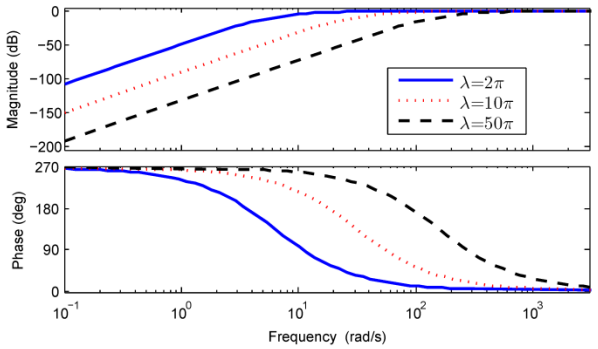

FIGURE 3. Frequency characteristics of $G_1(s)$ of the 3rd–order EDO with different bandwidths.

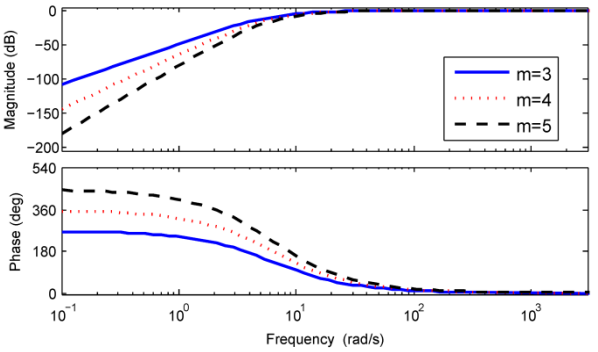

FIGURE 4. Frequency characteristics of $G_1(s)$ of EDO of different orders with fixed bandwidth ($\lambda = 2\pi$ rad/s).

From Fig. 3 and Fig. 4, it can be concluded that the lumped disturbance can be estimated by EDO precisely only if the bandwidth of EDO is much more than the frequency content of the disturbance. Furthermore, higher order of EDO will bring higher precision in disturbance estimate when the bandwidth is fixed. In order to estimate the dynamic imbalance disturbance with the same frequency as high-speed rotor effectively, higher bandwidth should be chosen for EDO. However, higher bandwidth increases the sensitivity to noises in measurement [39], and will lead to the problem of high gains.

IV. DESIGN AND ANALYSIS OF EHDO

To avoid the problems of EDO, an EHDO is proposed for the disturbance model with harmonics in this section. The performance of EHDO is also discussed for the proposed tuning rules of the observer gains.

A. HARMONIC BASED DISTURBANCE MODEL

According to the performance analysis of EDO in Section III, it is known that the rotor dynamic imbalance disturbance is the dominant factor leading to high-gain problem since it has the same frequency as the rotor. To avoid the high-gain

problem resulting from the rotor dynamic imbalance, it can be expressed as a harmonic model embedded into the model describing the dynamics of the lumped disturbance since it has known frequency but unknown amplitude and phase.

Let $x_a = T_r$, $x_b = \dot{T}_r$, then the following equation can be derived from (5) as

$$\dot{x}_b = -u_r\Omega^4 \sin(\Omega t + \phi_d) = -\Omega^2 x_a \tag{17}$$

For the other disturbances $(d-T_r)$ in (3) except for the rotor dynamic imbalance, they can be regarded as slowly-varying disturbances and approximated by using an $(m-2)$th-order $(m \geq 3)$ polynomial. Let $x_1 = d - T_r$, $x_2 = \dot{x}_1, \cdots, x_{m-2} = \delta(t)$, then we have

$$\begin{cases} \dot{x}_a = x_b, \ \dot{x}_b = -\Omega^2 x_a \\ \dot{x}_j = x_{j+1}, \ j = 1, 2, \cdots, m-3 \\ \dot{x}_{m-2} = \delta\left(t\right) \end{cases} \tag{18}$$

where $\delta(t)$ denotes the $(m-2)$th-order derivative of $(d-T_r)$ which also represents the uncertainty in the mth-order model in (18). For convenience, $\delta(t)$ is supposed to be bounded.

According to the definition of the states in (18), the virtual measurement equation can be written as

$$d = x_a + x_1 \tag{19}$$

Let

$$\boldsymbol{x} = \begin{bmatrix} x_a \\ x_b \\ x_1 \\ \vdots \\ x_{m-3} \\ x_{m-2} \end{bmatrix}, \quad \boldsymbol{A} = \left[\begin{array}{cc:ccc} 0 & 1 & 0 & 0 & \cdots & 0 \\ -\Omega^2 & 0 & 0 & 0 & \cdots & 0 \\ \hdashline 0 & 0 & 0 & 1 & \cdots & 0 \\ \vdots & \vdots & \vdots & \vdots & \ddots & \vdots \\ 0 & 0 & 0 & 0 & \cdots & 1 \\ 0 & 0 & 0 & 0 & \cdots & 0 \end{array}\right],$$

$$\boldsymbol{B} = \begin{bmatrix} 0 & 0 & 0 & \cdots & 0 & 1 \end{bmatrix}^{\mathrm{T}}, \quad \boldsymbol{C} = \begin{bmatrix} 1 & 0 & 1 & \cdots & 0 & 0 \end{bmatrix},$$

then the disturbance model in (18) and (19) can be written in a compact form as

$$\begin{cases} \dot{\boldsymbol{x}} = \boldsymbol{A}\boldsymbol{x} + \boldsymbol{B}\delta\left(t\right) \\ d = \boldsymbol{C}\boldsymbol{x} \end{cases} \tag{20}$$

Since the pair $(\boldsymbol{A}, \boldsymbol{C})$ is observable, we can design an observer to estimate the disturbances.

B. DESIGN OF EHDO

Let $\hat{\boldsymbol{x}}$ and $\hat{d}$ represent the estimate of $\boldsymbol{x}$ and the prediction of d respectively, then an observer for (20) can be designed as

$$\begin{cases} \dot{\hat{\boldsymbol{x}}} = \boldsymbol{A}\hat{\boldsymbol{x}} + \boldsymbol{L}(d - \hat{d}) \\ \hat{d} = \boldsymbol{C}\hat{\boldsymbol{x}} \end{cases} \tag{21}$$

where $\boldsymbol{L}$ is an observer gain matrix. Substituting (7) into the first equation of (21) gives

$$\dot{\hat{\boldsymbol{x}}} = (\boldsymbol{A} - \boldsymbol{L}\boldsymbol{C})\hat{\boldsymbol{x}} + \boldsymbol{L}(T_e - J\dot{\omega} - D\omega) \tag{22}$$

Similar to the design of EDO, an auxiliary variable is also introduced to avoid the calculation of the angular acceleration. The auxiliary variable $\boldsymbol{z}$ is defined such that

$$\hat{\boldsymbol{x}} = \boldsymbol{z} - \boldsymbol{L}J\omega \tag{23}$$

According to (23), (22) can be rewritten as

$$\dot{\boldsymbol{z}} = (\boldsymbol{A} - \boldsymbol{L}\boldsymbol{C})\left(\boldsymbol{z} - \boldsymbol{L}J\omega\right) + \boldsymbol{L}\left(T_e - D\omega\right) \tag{24}$$

Thus, the EHDO is obtained in (23) and (24). Next, the convergence of EHDO will be analyzed.

The estimate errors $\tilde{\boldsymbol{x}} = \boldsymbol{x} - \hat{\boldsymbol{x}}$, $\tilde{d} = d - \hat{d}$, then the error dynamics of EHDO can be derived from (20) and (21) as

$$\begin{cases} \dot{\tilde{\boldsymbol{x}}} = (\boldsymbol{A} - \boldsymbol{L}\boldsymbol{C})\,\tilde{\boldsymbol{x}} + \boldsymbol{B}\delta\left(t\right) \\ \tilde{d} = \boldsymbol{C}\tilde{\boldsymbol{x}} \end{cases} \tag{25}$$

Since the pair $(\boldsymbol{A}, \boldsymbol{C})$ is observable, the matrix $(\boldsymbol{A}-\boldsymbol{L}\boldsymbol{C})$ can be Hurwitz by choosing suitable gain matrix $\boldsymbol{L}$. Then, given any positive definite matrix $\boldsymbol{Q}$, there exists a unique positive definite matrix $\boldsymbol{P}$ such that

$$(\boldsymbol{A} - \boldsymbol{L}\boldsymbol{C})^{\mathrm{T}}\boldsymbol{P} + \boldsymbol{P}(\boldsymbol{A} - \boldsymbol{L}\boldsymbol{C}) = -\boldsymbol{Q} \tag{26}$$

For the error dynamics in (25), choose Lyapunov candidate function as

$$V_0 = \tilde{\boldsymbol{x}}^{\mathrm{T}}\boldsymbol{P}\tilde{\boldsymbol{x}} > 0 \tag{27}$$

Taking the time derivative of V_0 along (25) and (26) gives

$$\begin{aligned} \dot{V}_0 &= \dot{\tilde{\boldsymbol{x}}}^{\mathrm{T}}\boldsymbol{P}\tilde{\boldsymbol{x}} + \tilde{\boldsymbol{x}}^{\mathrm{T}}\boldsymbol{P}\dot{\tilde{\boldsymbol{x}}} \\ &= \tilde{\boldsymbol{x}}^{\mathrm{T}}[(\boldsymbol{A} - \boldsymbol{L}\boldsymbol{C})^{\mathrm{T}}\boldsymbol{P} + \boldsymbol{P}(\boldsymbol{A} - \boldsymbol{L}\boldsymbol{C})]\tilde{\boldsymbol{x}} + 2\tilde{\boldsymbol{x}}^{\mathrm{T}}\boldsymbol{P}\boldsymbol{B}\delta(t) \\ &= -\tilde{\boldsymbol{x}}^{\mathrm{T}}\boldsymbol{Q}\tilde{\boldsymbol{x}} + 2\tilde{\boldsymbol{x}}^{\mathrm{T}}\boldsymbol{P}\boldsymbol{B}\delta(t) \end{aligned} \tag{28}$$

Let λ_p, λ_q, and δ_m denote the maximal eigenvalue of $\boldsymbol{P}$, the minimal eigenvalue of $\boldsymbol{Q}$, and the upper bound of $\delta(t)$ respectively, then the following equality can be derived from (28) as

$$\begin{aligned} \dot{V}_0 &\leq -\lambda_q \left\|\tilde{\boldsymbol{x}}\right\|^2 + 2\left\|\tilde{\boldsymbol{x}}\right\| \left\|\boldsymbol{P}\right\| \left\|\boldsymbol{B}\right\| \delta_m \\ &= -\lambda_q \left\|\tilde{\boldsymbol{x}}\right\|^2 + 2\lambda_p\delta_m \left\|\tilde{\boldsymbol{x}}\right\| \end{aligned} \tag{29}$$

where $||\cdot||$ denotes 2-norm of a vector or a matrix.

From (29), it is known that the estimate error of EHDO is bounded. When $\|\tilde{\boldsymbol{x}}\| > 2\lambda_p\delta_m/\lambda_q$, $\dot{V}_0 < 0$ which will drive the trajectory of $\tilde{\boldsymbol{x}}$ into a bounded region $\boldsymbol{R}_1 = \{\tilde{\boldsymbol{x}} | \|\tilde{\boldsymbol{x}}\| \leq 2\lambda_p\delta_m/\lambda_q\}$. The upper bound of $\boldsymbol{R}_1$ depends on λ_p, λ_q and δ_m, and it can be decreased by regulating the gain matrix $\boldsymbol{L}$.

C. ANALYSIS OF EHDO

Similar to EDO, the performance of EHDO is also analyzed. Let $\boldsymbol{L} = \begin{bmatrix} l_a & l_b & l_1 & \cdots & l_{m-2} \end{bmatrix}^{\mathrm{T}}$, (21) can be rewritten as

$$\begin{cases} \dot{\hat{x}}_a = \hat{x}_b + l_a\tilde{d} \\ \dot{\hat{x}}_b = -\Omega^2\hat{x}_a + l_b\tilde{d} \\ \dot{\hat{x}}_j = \hat{x}_{j+1} + l_j\tilde{d}, \quad j = 1, 2, \cdots, m-3 \\ \dot{\hat{x}}_{m-2} = l_{m-2}\tilde{d} \end{cases} \tag{30}$$

According to (30), we can get

$$\begin{cases} \ddot{\hat{x}}_a + \Omega^2\hat{x}_a = -l_a\dot{\tilde{d}} - l_b\tilde{d} \\ \hat{x}_1^{(m-2)} = l_1\tilde{d}^{(m-3)} + l_2\tilde{d}^{(m-4)} + \cdots + l_{m-2}\tilde{d} \end{cases} \tag{31}$$

Under zero initial conditions, the Laplace transform expression of (31) can be written as

$$\begin{cases} \hat{x}_a(s) = \dfrac{l_a s + l_b}{s^2 + \Omega^2}\tilde{d}(s) \\ \hat{x}_1(s) = \dfrac{l_1 s^{m-3} + l_2 s^{m-4} + \cdots + l_{m-2}}{s^{m-2}}\tilde{d}(s) \end{cases} \tag{32}$$

Since $d(s) = \hat{d}(s) + \tilde{d}(s) = \hat{x}_a(s) + \hat{x}_1(s) + \tilde{d}(s)$, the transfer function from the lumped disturbance d to the estimate error $\tilde{d}$ can be derived from (32) as

$$G_2(s) = \frac{s^{m-2}(s^2+\Omega^2)}{s^{m-2}(l_a s+l_b)+(s^2+\Omega^2)(s^{m-2}+l_1 s^{m-3}+\cdots l_{m-2})} \tag{33}$$

From (33), the characteristic polynomial can be written as

$$D(s) = s^{m-2}(l_a s+l_b)+(s^2+\Omega^2)(s^{m-2}+l_1 s^{m-3}+\cdots l_{m-2}) \tag{34}$$

If the bandwidth of EHDO is chosen as $\lambda > 0$ and the poles of (33) are configured as $(m-2)$-times multiple real roots of $-\lambda$ and a pair of conjugate roots of $-\lambda \pm j\Omega$, the characteristic polynomial can be given by

$$D(s) = (s+\lambda)^{m-2}[(s+\lambda)^2 + \Omega^2] \tag{35}$$

Comparing (34) with (35), then the observer gains are the solutions to the algebraic equations as follows:

$$\begin{cases} l_1 + l_a = m\lambda \\ l_2 + l_b = C_m^2\lambda^2 \\ l_{i+2} + l_i\Omega^2 = C_m^{i+2}\lambda^{i+2} + C_{m-2}^{i}\lambda^i\Omega^2 \\ l_{m-3} = m\lambda^{m-1}/\Omega^2 + (m-2)\lambda^{m-3} \\ l_{m-2} = \lambda^m/\Omega^2 + \lambda^{m-2} \end{cases} \tag{36}$$

where $C_m^n = m!/(n!\,(m-n)!)$, $n \le m$ is a positive integer, $i = 1, 2, \cdots, m-4$.

By using the observer gains derived from (36), the frequency characteristics of $G_2(s)$ can be plotted to demonstrate the effects of different bandwidths and different orders on the performance of EHDO. Assuming that the rotor velocity $\Omega = 200\pi$ rad/s, the frequency responses of $G_2(s)$ for EHDO with different bandwidths ($\lambda = 2\pi$, 10π, 50π rad/s) and different orders ($m = 3, 4, 5$) are depicted in Fig. 5 and Fig. 6 respectively.

From Fig. 5 and Fig. 6, it is known that the rotor dynamic imbalance disturbance with the angular frequency of 200π rad/s can be estimated precisely by EHDO even with a low bandwidth. Meanwhile, the other disturbances with lower frequency content also can be estimated precisely. Thus, high gains are not necessary in EHDO and the high-gain problem of EDO can be avoided. Similar to EDO, the estimation accuracy of disturbance also can be improved by EHDO with the increase of the order or bandwidth.

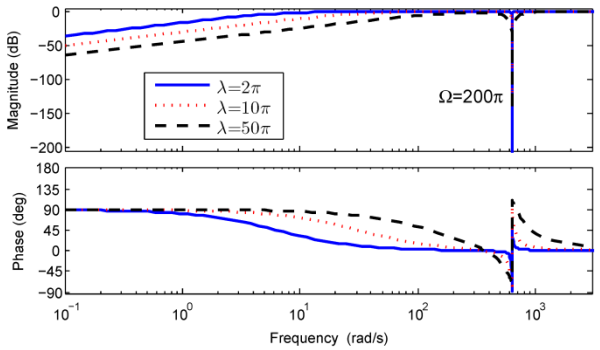

FIGURE 5. Frequency characteristics of $G_2(s)$ of the 3rd–order EHDO with different bandwidths.

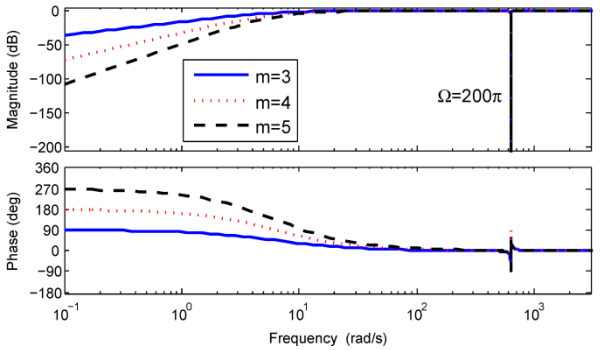

FIGURE 6. Frequency characteristics of $G_2(s)$ of EHDO of different orders with fixed bandwidth ($\lambda = 2\pi$ rad/s).

V. EHDO BASED GIMBAL CONTROLLER

Based on the EHDO designed in Section IV, a gimbal controller can be designed for the gimbal servo system described by (1)-(3) via backstepping method. The design procedure is divided into 3 steps:

Step 1: Design a gimbal speed controller to track the desired speed ω_d for (3) by using the electromagnetic torque T_e as virtual control input;

Step 2: Resolve the desired torque T_e^* into current command in d-q reference coordinate according to (2);

Step 3: Design current controller to track the current command according to (1).

Step 1: Gimbal speed controller design

Let T_e^* denote the desired electromagnetic torque and define speed tracking error as $\tilde{\omega} = \omega_d - \omega$ and torque error as $\tilde{T}_e = T_e^* - T_e$, then the following error equation can be derived from (3) as

$$\begin{aligned} J\dot{\tilde{\omega}} &= J\dot{\omega}_d - J\dot{\omega} \\ &= J\dot{\omega}_d - T_e + d + D\omega \\ &= J\dot{\omega}_d - T_e^* + T_e^* - T_e + d + D(\omega_d - \tilde{\omega}) \\ &= -T_e^* + J\dot{\omega}_d + D\omega_d - D\tilde{\omega} + \tilde{T}_e + d \end{aligned} \tag{37}$$

For the error system in (37), choose Lyapunov candidate function as

$$V_1 = \frac{1}{2}J\tilde{\omega}^2 + V_0 > 0 \tag{38}$$

The time derivative of (38) along (37) can be expressed as

$$\begin{aligned}\dot{V}_1 &= J\tilde{\omega}\dot{\tilde{\omega}} + \dot{V}_0 \\ &= \tilde{\omega}(-T_e^* + J\dot{\omega}_d + D\omega_d - D\tilde{\omega} + \tilde{T}_e + d) + \dot{V}_0 \end{aligned} \quad (39)$$

If the virtual control T_e^* is designed as

$$T_e^* = J\dot{\omega}_d + D\omega_d + k_0\tilde{\omega} + \hat{d} \quad (40)$$

Then (39) can be rewritten as

$$\dot{V}_1 = -(k_0 + D)\tilde{\omega}^2 + \tilde{\omega}\tilde{T}_e + \tilde{\omega}\tilde{d} + \dot{V}_0 \quad (41)$$

where $k_0 > 0$. Let $k_0' = k_0 + D$, then (41) can be rewritten according to (29) and (25) as

$$\begin{aligned}\dot{V}_1 &\le -k_0'\tilde{\omega}^2 + \tilde{\omega}\tilde{T}_e + |\tilde{\omega}||\tilde{d}| - \lambda_q \|\tilde{\boldsymbol{x}}\|^2 + 2\lambda_p\delta_m \|\tilde{\boldsymbol{x}}\| \\ &\le -k_0'\tilde{\omega}^2 + \tilde{\omega}\tilde{T}_e + |\tilde{\omega}| \|C\| \|\tilde{\boldsymbol{x}}\| - \lambda_q \|\tilde{\boldsymbol{x}}\|^2 + 2\lambda_p\delta_m \|\tilde{\boldsymbol{x}}\| \\ &\le -k_0'\tilde{\omega}^2 + \tilde{\omega}\tilde{T}_e + \sqrt{2}|\tilde{\omega}| \|\tilde{\boldsymbol{x}}\| - \lambda_q \|\tilde{\boldsymbol{x}}\|^2 + 2\lambda_p\delta_m \|\tilde{\boldsymbol{x}}\| \end{aligned} \quad (42)$$

In (42), it is noted that $2|\tilde{\omega}| \|\tilde{\boldsymbol{x}}\| \le |\tilde{\omega}|^2 + \|\tilde{\boldsymbol{x}}\|^2$. Let $c_1 = k_0' - \sqrt{2}/2$, $c_2 = \lambda_q - \sqrt{2}/2$, then (42) can be changed into the following form as

$$\dot{V}_1 \le -c_1\tilde{\omega}^2 - c_2 \|\tilde{\boldsymbol{x}}\|^2 + 2\lambda_p\delta_m \|\tilde{\boldsymbol{x}}\| + \tilde{\omega}\tilde{T}_e \quad (43)$$

From (43), it is known that the closed-loop system is asymptotically bounded by using the virtual control in (40) if the torque error $\tilde{T}_e = 0$. Therefore, the next work is to design current controller to realize the desired torque T_e^* in (40).

Step 2: Current command generator

In order to track the desired torque T_e^* for PMSM in the gimbal servo system in Fig. 2, it should be resolved into the current command i_d^* and i_q^* according to the torque equation in d-q frame. Since $L_d = L_q = L$ for surface-mounted PMSMs, (2) can be rewritten by defining $k_t = 1.5n_p\psi_f$ as

$$T_e = k_t i_q \quad (44)$$

According to (44), the torque command T_e^* can be transformed into the current command as

$$\begin{cases} i_d^* = 0 \\ i_q^* = T_e^*/k_t \end{cases} \quad (45)$$

According to (44) and (45), the torque error $\tilde{T}_e$ also can be obtained as

$$\tilde{T}_e = k_t(i_q^* - i_q) \quad (46)$$

Step 3: Current controller design.

In order to track the current command in (45), current controller will be designed in d-q frame. Define current errors as $\tilde{i}_d = i_d^* - i_d$ and $\tilde{i}_q = i_q^* - i_q$, then the error equation can be derived from (1) as

$$\begin{cases} L_d\dot{\tilde{i}}_d = L_d p i_d^* - u_d + Ri_d - n_p\omega L_d i_q \\ L_q\dot{\tilde{i}}_q = L_q p i_q^* - u_q + Ri_q + n_p\omega L_q i_d + n_p\omega\psi_f \end{cases} \quad (47)$$

Choose Lyapunov candidate function as

$$V_2 = V_1 + \frac{1}{2}L_d\tilde{i}_d^2 + \frac{1}{2}L_q\tilde{i}_q^2 > 0 \quad (48)$$

Taking the time derivative of V_2 along (43) gives

$$\begin{aligned}\dot{V}_2 &= \dot{V}_1 + L_d\tilde{i}_d\dot{\tilde{i}}_d + L_q\tilde{i}_q\dot{\tilde{i}}_q \\ &\le -c_1\tilde{\omega}^2 - c_2 \|\tilde{\boldsymbol{x}}\|^2 + 2\lambda_p\delta_m \|\tilde{\boldsymbol{x}}\| \\ &\quad + \tilde{\omega}\tilde{T}_e + L_d\tilde{i}_d\dot{\tilde{i}}_d + L_q\tilde{i}_q\dot{\tilde{i}}_q \end{aligned} \quad (49)$$

Let k_1 and k_2 are positive constants, then we can design current controller as

$$\begin{cases} u_d = L_d p i_d^* + Ri_d^* - n_p\omega L_d i_q + k_1\tilde{i}_d \\ u_q = L_q p i_q^* + Ri_q^* + n_p\omega L_q i_d + n_p\omega\psi_f + k_t\tilde{\omega} + k_2\tilde{i}_q \end{cases} \quad (50)$$

According to (50) and (45), (47) can be rewritten as

$$\begin{cases} L_d\dot{\tilde{i}}_d = -(k_1 + R)\tilde{i}_d \\ L_q\dot{\tilde{i}}_q = -(k_2 + R)\tilde{i}_q - k_t\tilde{\omega} \end{cases} \quad (51)$$

Let $c_3 = k_1 + R$, $c_4 = k_2 + R$, then (51) can be modified according to (46) as

$$\begin{cases} L_d\dot{\tilde{i}}_d\tilde{i}_d = -c_3\tilde{i}_d^2 \\ L_q\dot{\tilde{i}}_q\tilde{i}_q = -c_4\tilde{i}_q^2 - \tilde{\omega}\tilde{T}_e \end{cases} \quad (52)$$

Substituting (52) into (49) gives

$$\dot{V}_2 \le -c_1\tilde{\omega}^2 - c_2 \|\tilde{\boldsymbol{x}}\|^2 + 2\lambda_p\delta_m \|\tilde{\boldsymbol{x}}\| - c_3\tilde{i}_d^2 - c_4\tilde{i}_q^2 \quad (53)$$

Let $\boldsymbol{e} = [\tilde{\omega}, \tilde{\boldsymbol{x}}^T, \tilde{i}_d, \tilde{i}_q]^T$, $c = \min\{c_1, c_2, c_3, c_4\}$, then (53) can be enlarged into the following form as

$$\begin{aligned}\dot{V}_2 &\le -c[\tilde{\omega}^2 + \|\tilde{\boldsymbol{x}}\|^2 + \tilde{i}_d^2 + \tilde{i}_q^2] + 2\lambda_p\delta_m \|\tilde{\boldsymbol{x}}\| \\ &\le -c \|\boldsymbol{e}\|^2 + 2\lambda_p\delta_m \|\boldsymbol{e}\| \end{aligned} \quad (54)$$

From (54), it can be concluded that the closed-loop system is asymptotically bounded. When $\|\boldsymbol{e}\| > 2\lambda_p\delta_m/c$, $\dot{V}_2 < 0$, it will drive the trajectory of $\boldsymbol{e}$ into a bounded region $\boldsymbol{R}_2 = \{\boldsymbol{e} | \|\boldsymbol{e}\| \le 2\lambda_p\delta_m/c\}$. The upper bound of $\boldsymbol{R}_2$ depends on c, λ_p and δ_m, and it can be decreased by regulating the observer bandwidth λ and the controller gains k_0, k_1, and k_2.

VI. SIMULATION AND EXPERIMENTAL RESULTS

In this section, simulations and experiments of EHDO and EDO with different orders for the gimbal servo system have been performed to demonstrate the effectiveness of the proposed EHDO and controller.

A. SIMULATION RESULTS

Gimbal servo control system is established in Matlab/Simulink and the performance of the system is analyzed in this section. The parameters of the gimbal servo system are listed in Table 1, where the values of the parameters are consistent with the actual experimental platform.

According to (4), the parameters of disturbance related to gimbal system are chosen as $T_{cog} = 0.1$Nm, $N_{co} = 48$, $T_{st} = 0.02$Nm, $T_c = 0.005$Nm, $\omega_s = 0.002$rad/s, respectively. Since the gimbal simulator is controlled to run by the gimbal drive circuit, T_{flux}, T_d and T_m have already existed in the system, so we do not need to set the parameter of T_{flux}, T_d and T_m additionally. The velocity of the CMG rotor

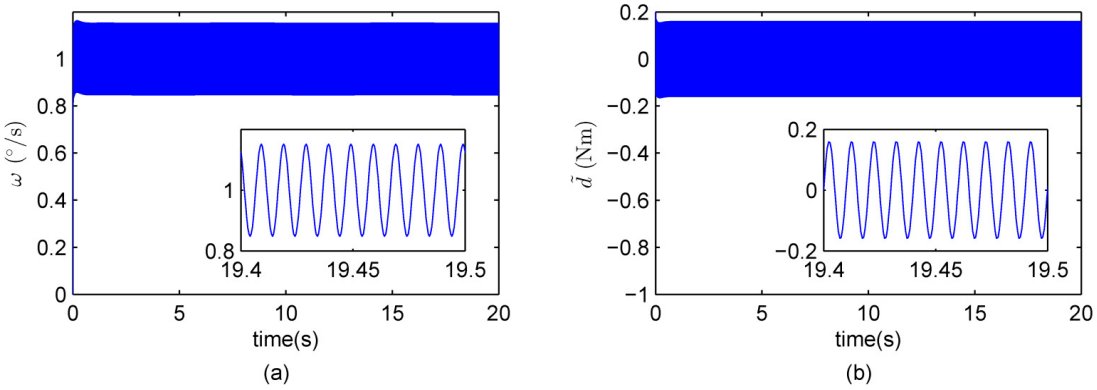

FIGURE 7. Simulation results of gimbal speed and disturbance estimate error for 3rd-order EDO. (a) Gimbal speed. (b) Disturbance estimate error.

TABLE 1. Parameters of gimbal servo system.

Parameters	Values
Moment of inertia	0.082 Kg.m^2
Damping coefficient	0.1 Nm/rad/s
Stator resistance	1 Ω
d-axis inductance	0.0098 H
q-axis inductance	0.0098 H
Pole pairs	6
Stator flux linkage	0.16 Wb

is 6000r/min, the quantity of rotor dynamic imbalance is $u_r = 4\text{g.cm}^2$, $\phi_d = 0°$, then the amplitude of the dynamic imbalance torque T_r can be calculated from (5). Disturbance torque caused by spacecraft motion is set as $T_s = 0.03\text{Nm}$.

The desired angular speed of gimbal is $\omega_d = 1°/\text{s}$. The parameters of speed and current controller are $k_0 = 30$, $k_1 = 20$, $k_2 = 20$, respectively.

By using the gimbal velocity ω and electromagnetic torque T_e, the EHDO in (24) and the EDO in (12) can be implemented with the bandwidth $\lambda = 2\pi\text{rad/s}$. To compare the performance of the EHDO and the EDO, and analyze the effects of different orders of the EHDO and the EDO on the disturbance estimate error, 3rd-order disturbance observer and 4th-order disturbance observer are considered in the simulation. The observer gains of the EHDO and EDO are calculated by (36) and (16), respectively.

Case 1: The 3rd-order disturbance observer.

In this case, the gains of observers are listed in Table 2, and simulation results for the 3rd-order EDO and the EHDO can be achieved. Fig. 7 and Fig. 8 show the gimbal angular speed and disturbance estimate errors of the 3rd-order EDO and the EHDO, respectively.

TABLE 2. Observer gains for 3rd-order EDO and EHDO.

	l_a	l_b	l_1	l_2	l_3
EDO	N/A	N/A	18.85	118.5	6
EHDO	12.57	118.4	6.284	N/A	N/A

Figs. 7(a) and 7(b) show the gimbal angular speed and the disturbance estimate error of the 3rd-order EDO. The gimbal servo speed fluctuates within 0.16°/s, and the disturbance estimate error is within 0.158Nm. It is clear that 3rd-order EDO is difficult to estimate the rotor dynamic imbalance disturbance since the bandwidth is much less than the frequency of rotor dynamic imbalance torque. Therefore the high-frequency component still exists in the disturbance estimate error, causing the high-frequency vibration in gimbal speed. On the other hand, the 3rd-order EDO uses the first three derivatives of disturbance for estimation, thus the estimate effect of low-frequency disturbance is improved.

From Fig. 8, it is known that the gimbal angular speed fluctuates within 0.025°/s, and the disturbance estimate error of the EHDO fluctuates within 0.02Nm. It is obvious that the control performance of gimbal servo system is improved as compared with the conventional 3rd-order EDO. However, since only the first derivative of low-frequency disturbances is used in the 3rd–order EHDO, the low-frequency component still exists in disturbance estimate error and gimbal angular speed.

Case 2: The 4th-order disturbance observer

Gains of the 4th–order EHDO and EDO are listed in Table 3. The gimbal angular speed and the disturbance estimate error of the 4th-order EDO and EHDO are shown in Figs. 9 and 10, respectively.

TABLE 3. Observer gains for 4th-order EDO and EHDO.

	l_a	l_b	l_1	l_2	l_3	l_4
EDO	N/A	N/A	25.13	236.9	992.2	1559
EHDO	12.56	197.4	12.57	39.48	N/A	N/A

Fig. 9(a) and Fig. 9(b) show the gimbal angular speed and the disturbance estimate error of the 4th-order EDO. The gimbal servo speed fluctuates within 0.16°/s, and the disturbance estimate error is within 0.158Nm. The EDO still cannot estimate rotor dynamic imbalance disturbance since the bandwidth of observer is less than disturbance frequency.

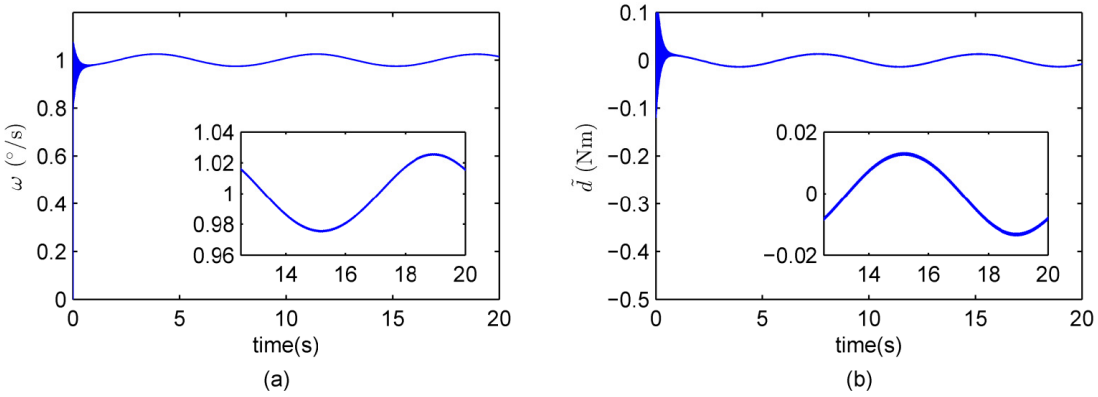

FIGURE 8. Simulation results of gimbal speed and disturbance estimate error for 3rd-order EHDO. (a) Gimbal speed. (b) Disturbance estimate error.

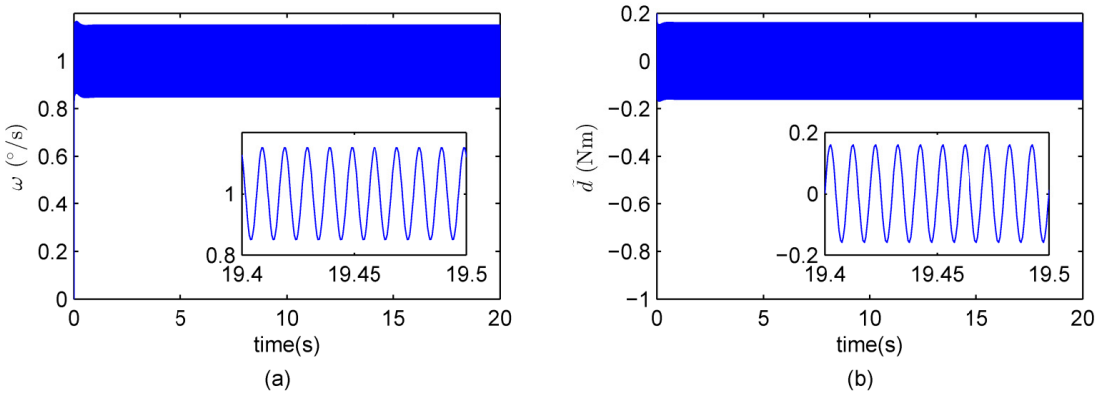

FIGURE 9. Simulation results of gimbal speed and disturbance estimate error for 4th-order EDO. (a) Gimbal speed. (b) Disturbance estimate error.

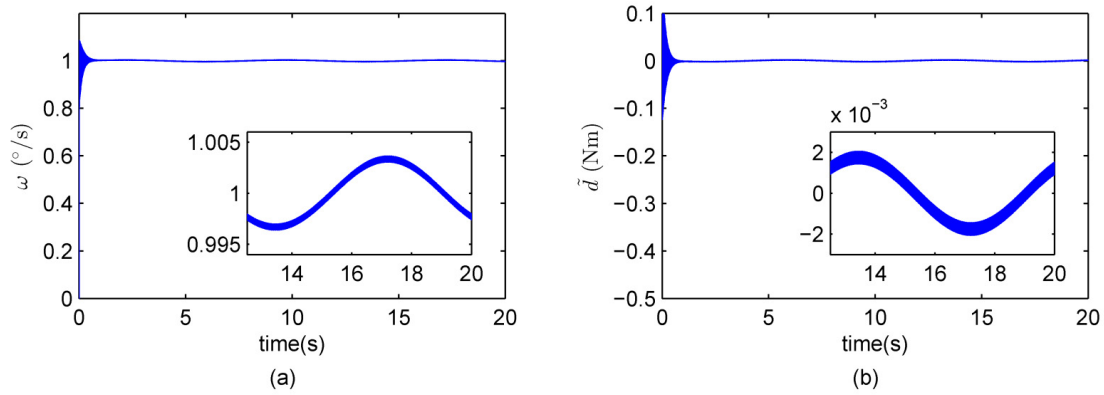

FIGURE 10. Simulation results of gimbal speed and disturbance estimate error for 4th-order EHDO. (a) Gimbal speed. (b) Disturbance estimate error.

Therefore the high-frequency component still exists in the disturbance estimate error, causing the high- frequency vibration in gimbal speed.

From Fig. 10(a) and Fig. 10(b), it is obvious that the estimate error is degraded with the order of the EHDO increases. The gimbal angular speed fluctuates within 0.005°/s, and the disturbance estimate error of the 4th–order EHDO fluctuates within 2×10^{-3}Nm, which is less than that of 3rd-order EHDO. Therefore, the control performance of gimbal servo system is improved as compared with the 3rd–order EHDO.

According to the simulation results, the standard deviation of gimbal angular speed is computed to evaluate the

TABLE 4. Standard derivation of gimbal speed in simulations.

	3rd-order	4th-order
EDO	0.1071°/s	0.1072°/s
EHDO	0.0179°/s	0.0024°/s

performance of the EDO and the EHDO, as shown in Table 4. It is obvious that the standard derivation of gimbal speed for EHDO is much lower than that for EDO, and it degrades as the order of EHDO increases.

B. EXPERIMENTAL RESULTS

In this section, semi-physical experiments were carried out to verify the effectiveness of the proposed EHDO and gimbal controller. The semi-physical experiment platform included a CMG gimbal simulator, gimbal drive and control circuits, an upper computer and power supplies, as shown in Figure 11.

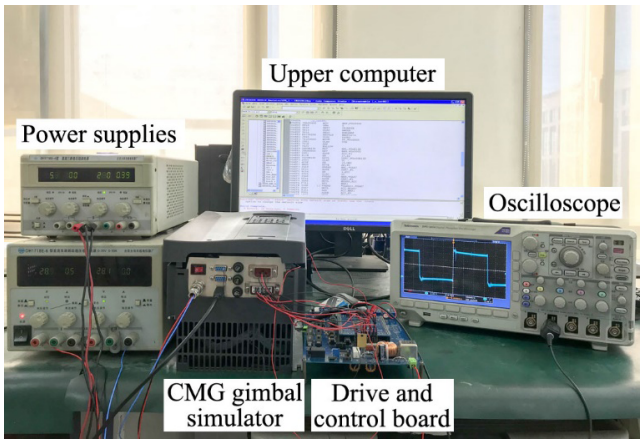

FIGURE 11. Simi-physical experiment platform.

CMG gimbal simulator is an electric load which has similar electrical and mechanical characteristics to practical CMG gimbal motor. CMG gimbal simulator can be used as a substitute for the real CMG gimbal system and it has been used to test CMG drive circuits in spacecraft engineering. By using CMG gimbal simulator, physical parameters of CMG gimbal and disturbances parameters such as friction and rotor imbalance could be preset by the upper computer. Therefore, it was convenient to evaluate the performance of the proposed EHDO by comparing the estimates with the preset values of disturbances. While a practical CMG gimbal system is used, the actual values of disturbances cannot be obtained.

Gimbal drive and control circuit is in charge of driving gimbal simulator. The signals of three-phase current are sampled and adjusted by signal acquisition module (ADS8568) and then transmitted to a digital signal processor (TMS320F28335). As the core of the drive and control circuit, the TMS320F28335 formulates the control signal according to the information of speed and current. Then, the proposed disturbance observer and control algorithm can be implemented in DSP with a sampling period of 125μs. The drive circuit of CMG gimbal simulator is a three-phrase full-bridge converter consisting of 6 MOSFETs (IRFR3910).

The parameters of the CMG gimbal servo system are consistent with simulations. Two cases that m =3 and 4 are considered in the experiment.

Case 1: The 3rd-order disturbance observer.

In this case, the gains of the 3rd-order EDO and EHDO are listed in Table 2. Fig. 12 and Fig. 13 show the gimbal angular speed and the estimate of disturbance for the 3rd-order EDO and the EHDO, respectively.

Considering the periodic perturbations in the estimate of disturbances, we show the experimental results from 10s to 17.5s to illustrate the performance of different disturbance observers with the order of 3.

As shown in Figs. 12(a) and 13(a), the gimbal speed for 3rd-order EDO and EHDO fluctuates within 0.2°/s and 0.11°/s, respectively. From Figs. 12(b) and 13(b), it is obvious that the rotor dynamic imbalance torque could not be estimated by the 3rd-order EDO, gimbal speed is affected by the rotor dynamic imbalance. Comparatively, the 3rd-order EHDO could estimate the rotor dynamic imbalance torque. However, using only the first derivative of T_g in 3rd-order EHDO will result in large model error, which leads to a decrease in the estimate accuracy of T_g. The gimbal speed for 3rd-order EHDO still contains a fluctuation with the same frequency as T_g.

Case 2: The 4th-order disturbance observer.

The gains of the 4th-order EDO and EHDO are listed in Table 3. The gimbal angular speed and the estimate of disturbance for the 4th-order EDO and EHDO are shown in Figs. 14 and 15, respectively.

As shown in Figs. 14(a) and 15(a), the gimbal speed for 4th-order EDO and EHDO fluctuates within 0.2°/s and 0.1°/s, respectively. From Figs. 14(b) and 15(b), it can be concluded that the 4th-order EDO still cannot estimate the rotor dynamic imbalance, while the 4th-order EHDO can estimate the rotor dynamic imbalance torque as well as the disturbance with lower frequency. Compared with the 3rd-order EHDO, the estimation accuracy of the 4th-order EHDO is improved since the model error of T_g is reduced. The accuracy of gimbal speed is improved through the feedforward compensation of disturbances. The fluctuation with the same frequency as T_g has been degraded in the gimbal speed.

The standard deviation of gimbal angular speed is shown in Table 5.

TABLE 5. Standard derivation of gimbal speed in experiments.

	3rd-order	4th-order
EDO	0.1197°/s	0.1198°/s
EHDO	0.0714°/s	0.0671°/s

In summary, the conventional EDO cannot estimate the high-frequency disturbance with a bandwidth much less than

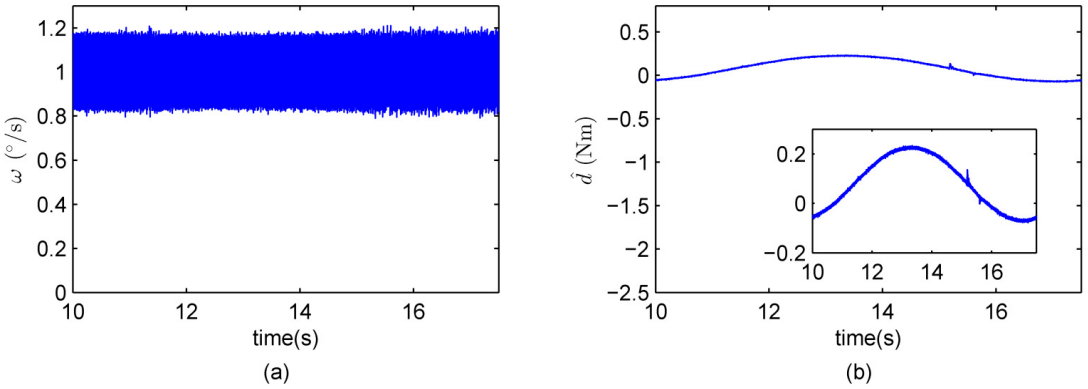

FIGURE 12. Experimental result of gimbal speed and disturbance estimate for 3rd-order EDO. (a) Gimbal speed. (b) Disturbance estimate.

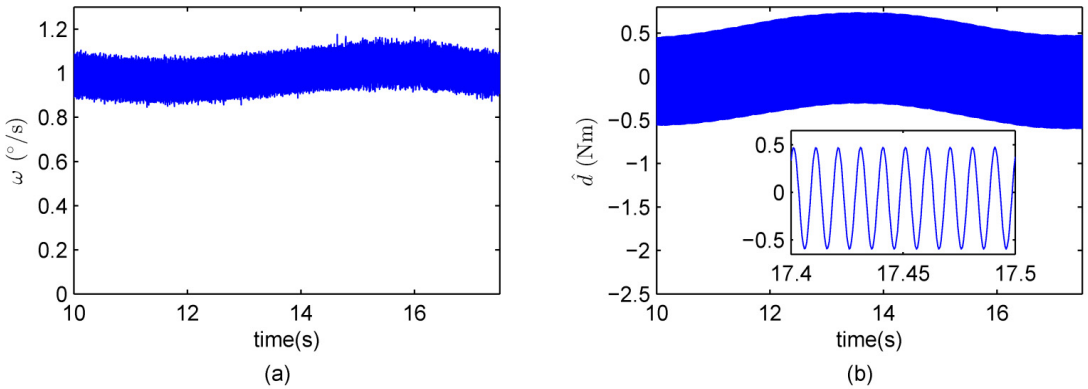

FIGURE 13. Experimental result of gimbal speed and disturbance estimate for 3rd-order EHDO. (a) Gimbal speed. (b) Disturbance estimate.

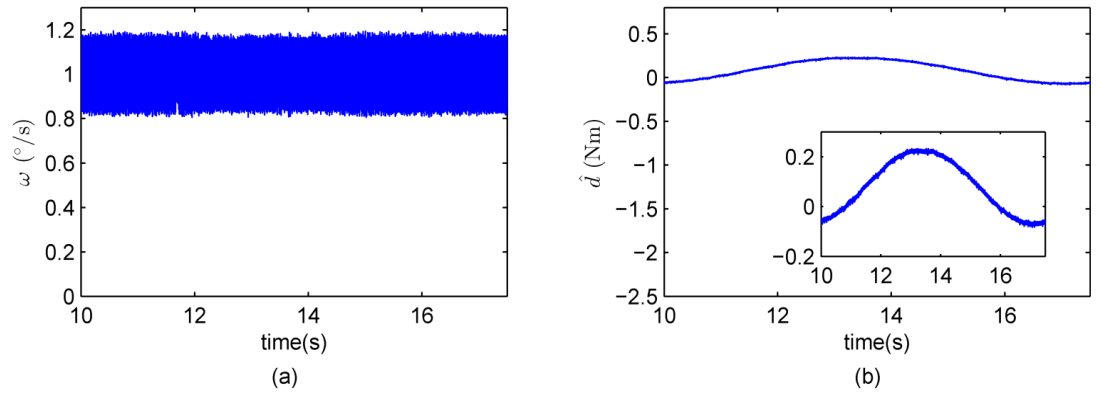

FIGURE 14. Experimental result of gimbal speed and disturbance estimate for 4th-order EDO. (a) Gimbal speed. (b) Disturbance estimate.

the frequency of disturbance. Compared with EDO, EHDO can estimate the lumped disturbance precisely even with a lower bandwidth. As shown in the simulation and experimental results, the estimation error decreases with the increase of the order of EHDO. Moreover, the proposed EHDO can avoid the high gain problem in EDO. By compensating multiple disturbances in gimbal servo systems with the estimate of the EHDO, the disturbances can be rejected significantly and the expected control performance of gimbal speed control can be achieved.

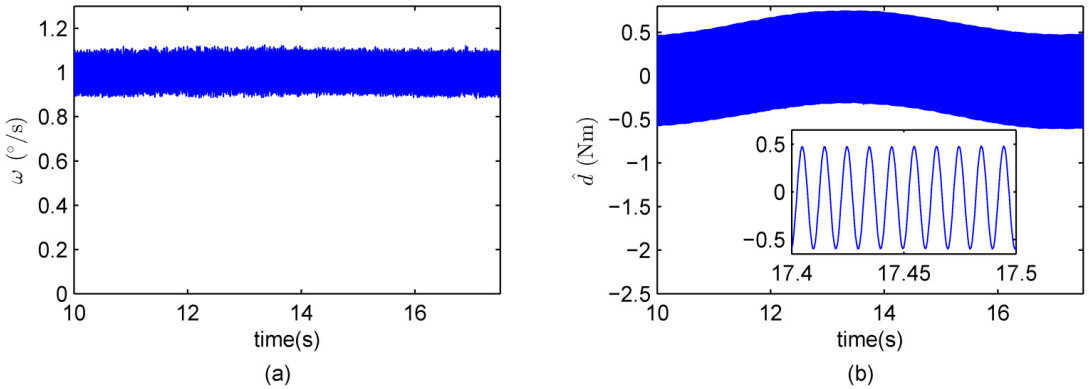

FIGURE 15. Experimental result of gimbal speed and disturbance estimate for 4th-order EHDO. (a) Gimbal speed. (b) Disturbance estimate.

VII. CONCLUSION

In this paper, an EHDO is proposed to estimate the multiple disturbances described by a second-order harmonic model and $(m-2)$th-order polynomial model in gimbal servo system. This observer can estimate the rotor dynamic imbalance disturbance and other slowly-varying disturbances precisely even with a lower bandwidth. Thereafter, feedforward is used to compensate multiple disturbances in gimbal servo systems by using estimated disturbance from EHDO, and a backstepping based composite controller is designed to achieve expected control performance in gimbal speed control for CMGs. Simulation and experimental results are presented to demonstrate the effectiveness of the EHDO and the composite speed controller. The proposed EHDO and the composite controller can be applied in the development of CMG engineering. Since periodic disturbances and uncertainties widely exist in practical engineering, it is hoped that the proposed EHDO and composite controller can be extended to other systems in the future.

REFERENCES

[1] C. J. Heiberg, D. Bailey, and B. Wie, "Precision spacecraft pointing using single-gimbal control moment gyroscopes with disturbance," *J. Guid., Control Dyn.*, vol. 21, no. 1, pp. 77–85, Jan.-Feb. 2000.
[2] S. P. Bhat and P. K. Tiwari, "Controllability of spacecraft attitude using control moment gyroscopes," *IEEE Trans. Autom. Control*, vol. 54, no. 3, pp. 585–590, Mar. 2009.
[3] R. Yan and Z. Wu, "Attitude stabilization of flexible spacecrafts via extended disturbance observer based controller," *Acta Astronaut.*, vol. 133, pp. 73–80, Apr. 2017.
[4] Y. Kusuda and M. Takahashi, "Feedback control with nominal inputs for agile satellites using control moment gyros," *J. Guid., Control Dyn.*, vol. 34, no. 4, pp. 1209–1218, Jul./Aug. 2011.
[5] Y. Xia, L. Dai, M. Fu, C. Li, and C. Wang, "Application of active disturbance rejection control in tank gun control system," *J. Franklin Inst.*, vol. 351, no. 4, pp. 2299–2314, Apr. 2014.
[6] S. Sung, G. Jang, and K. Kang, "Noise and vibration due to rotor eccentricity in a HDD spindle system," *Microsyst. Technol.*, vol. 20, nos. 8–9, pp. 1461–1469, 2014, doi: 10.1007/s00542-014-2139-2.
[7] Y. Zhang and J. Zhang, "Disturbance characteristics analysis of CMG due to imbalances and installation errors," *IEEE Trans. Aerosp. Electron. Syst.*, vol. 50, no. 2, pp. 1017–1026, Apr. 2014.
[8] Z. Wei, D. Li, Q. Luo, and J. Jiang, "Performance analysis of a flywheel microvibration isolation platform for spacecraft," *J. Spacecraft Rockets*, vol. 52, no. 4, pp. 1263–1268, Jul.-Aug. 2015.
[9] Q. Luo, D. Li, and J. Jiang, "Analysis and optimization of microvibration isolation for multiple flywheel systems of spacecraft," *AIAA J.*, vol. 54, no. 5, pp. 1719–1731, May 2016.
[10] X. Xu and S. Chen, "Field balancing and harmonic vibration suppression in rigid AMB-rotor systems with rotor imbalances and sensor runout," *Sensors*, vol. 15, no. 9, pp. 21876–21897, Aug. 2015.
[11] M. C. Chou, C. M. Liaw, S. B. Chien, F. H. Shieh, J. R. Tsai, and H. C. Chang, "Robust current and torque controls for PMSM driven satellite reaction wheel," *IEEE Trans. Aerosp. Electron. Syst.*, vol. 47, no. 1, pp. 58–74, Jan. 2011.
[12] Z. Wang, Z. Wu, and Y. Du, "Robust adaptive backstepping control for reentry reusable launch vehicles," *Acta Astronaut.*, vol. 126, pp. 258–264, Sep./Oct. 2016.
[13] S. Pan, J.-H. Zhang, and W.-Q. Huang, "Robust controller design of SGCMG driven by hollow USM," *Microsyst. Technol.*, vol. 22, no. 4, pp. 741–746, 2016, doi: 10.1007/s00542-015-2422-x.
[14] K. Jezernik, J. Korelič, and R. Horvat, "PMSM sliding mode FPGA-based control for torque ripple reduction," *IEEE Trans. Power Electron.*, vol. 28, no. 7, pp. 3549–3556, Jul. 2013.
[15] T. Kamel, D. Abdelkader, B. Said, S. Padmanaban, and A. Iqbal, "Extended Kalman filter based sliding mode control of parallel-connected two five-phase PMSM drive system," *Electronics*, vol. 7, no. 2, p. 14, 2018, doi: 10.3390/electronics7020014.
[16] M.-S. Wang and T.-M. Tsai, "Sliding mode and neural network control of sensorless PMSM controlled system for power consumption and performance improvement," *Energies*, vol. 10, no. 11, p. 1780, 2017, doi: 10.3390/en10111780.
[17] X. Sun, Z. Shi, L. Chen, and Z. Yang, "Internal model control for a bearingless permanent magnet synchronous motor based on inverse system method," *IEEE Trans. Energy Convers.*, vol. 31, no. 4, pp. 1539–1548, Dec. 2016.
[18] Y. Joo, G. Park, J. Back, and H. Shim, "Embedding internal model in disturbance observer with robust stability," *IEEE Trans. Autom. Control*, vol. 61, no. 10, pp. 3128–3133, Oct. 2016.
[19] P. Cui, S. Li, Q. Wang, Q. Gao, J. Cui, and H. Zhang, "Harmonic current suppression of an AMB rotor system at variable rotation speed based on multiple phase-shift notch filters," *IEEE Trans. Ind. Electron.*, vol. 63, no. 11, pp. 6962–6969, Nov. 2016.
[20] X. Sun, B. Su, L. Chen, Z. Yang, X. Xu, and Z. Shi, "Precise control of a four degree-of-freedom permanent magnet biased active magnetic bearing system in a magnetically suspended direct-driven spindle using neural network inverse scheme," *Mech. Syst. Signal Process.*, vol. 88, pp. 36–48, May 2017.
[21] X. Sun, L. Chen, H. Jiang, Z. Yang, J. Chen, and W. Zhang, "High-performance control for a bearingless permanent-magnet synchronous motor using neural network inverse scheme plus internal model controllers," *IEEE Trans. Ind. Electron.*, vol. 63, no. 6, pp. 3479–3488, Jun. 2016.
[22] W. Chen, J. Yang, L. Guo, and S. Li, "Disturbance-observer-based control and related methods-an overview," *IEEE Trans. Ind. Electron.*, vol. 63, no. 2, pp. 1083–1095, Feb. 2016.

[23] J. Yang, W.-H. Chen, S. Li, L. Guo, and Y. Yan, "Disturbance/uncertainty estimation and attenuation techniques in PMSM drives—A survey," *IEEE Trans. Ind. Electron.*, vol. 64, no. 4, pp. 3273–3285, Apr. 2017.
[24] W.-H. Chen, "Disturbance observer based control for nonlinear systems," *IEEE/ASME Trans. Mechatronics*, vol. 9, no. 4, pp. 706–710, Dec. 2004.
[25] J. Yang, S. Li, and X. Yu, "Sliding-mode control for systems with mismatched uncertainties via a disturbance observer," *IEEE Trans. Ind. Electron.*, vol. 60, no. 1, pp. 160–169, Jan. 2013.
[26] Z. Wang and Z. Wu, "Nonlinear attitude control scheme with disturbance observer for flexible spacecrafts," *Nonlinear Dyn.*, vol. 81, nos. 1–2, pp. 257–264, Jul. 2015.
[27] J. Han, "From PID to active disturbance rejection control," *IEEE Trans. Ind. Electron.*, vol. 56, no. 3, pp. 900–906, Mar. 2009.
[28] J. Han, "A class of extended state observers for uncertain systems," (in Chinese), *Control Decis.*, vol. 10, no. 1, pp. 85–88, Jan. 1995.
[29] G. Herbst, "A Simulative study on active disturbance rejection control (ADRC) as a control tool for practitioners," *Electronics*, vol. 2, no. 3, pp. 246–279, 2013, doi: 10.3390/electronics2030246.
[30] A. G. Wu, G. R. Duan, J. Dong, and Y. M. Fu, "Design of proportional-integral observers for discrete-time descriptor linear systems," *IET Control Theory Appl.*, vol. 3, no. 1, pp. 79–87, Jan. 2009.
[31] H. Li, X. Ning, and B. Han, "Speed tracking control for the gimbal system with harmonic drive," *Control Eng. Pract.*, vol. 58, pp. 204–213, Jan. 2017.
[32] R. D. Yan and Z. Wu, "Finite-time attitude stabilization of flexible spacecrafts via reduced-order sliding mode disturbance observer and nonsingular terminal sliding mode controller," *J. Aerosp. Eng.*, vol. 31, no. 4, p. 04018023, Jul. 2018.
[33] C. Dai, J. Yang, Z. Wang, and S. Li, "Universal active disturbance rejection control for non-linear systems with multiple disturbances via a high-order sliding mode observer," *IET Control Appl.*, vol. 11, no. 8, pp. 1194–1204, Dec. 2017.
[34] H. Kim, J. Son, and J. Lee, "A high-speed sliding-mode observer for the sensorless speed control of a PMSM," *IEEE Trans. Ind. Electron.*, vol. 58, no. 9, pp. 4069–4077, Sep. 2011.
[35] X. Zhang and Z. Li, "Sliding-mode observer-based mechanical parameter estimation for permanent magnet synchronous motor," *IEEE Trans. Power Electron.*, vol. 31, no. 8, pp. 5732–5745, Aug. 2016.
[36] K. Zhao, P. Li, C. Zhang, X. Li, J. He, and Y. L. Lin, "Sliding mode observer-based current sensor fault reconstruction and unknown load disturbance estimation for PMSM driven system," *Sensors*, vol. 17, no. 12, p. 2833, 2017, doi: 10.3390/s17122833.
[37] K.-S. Kim, K.-H. Rew, and S. Kim, "Disturbance observer for estimating higher order disturbances in time series expansion," *IEEE Trans. Autom. Control*, vol. 55, no. 8, pp. 1905–1911, Aug. 2010.
[38] D. Ginoya, P. D. Shendge, and S. B. Phadke, "Sliding mode control for mismatched uncertain systems using an extended disturbance observer," *IEEE Trans. Ind. Electron.*, vol. 61, no. 4, pp. 1983–1992, Apr. 2014.
[39] Q. Zheng, L. Q. Gao, and Z. Gao, "On validation of extended state observer through analysis and experimentation," *J. Dyn. Syst., Meas., Control*, vol. 134, no. 2, pp. 024505-1–024505-6, 2012.
[40] W.-H. Chen, "Harmonic disturbance observer for nonlinear systems," *J. Dyn. Syst., Meas. Control*, vol. 125, no. 1, pp. 114–117, Mar. 2003.
[41] Y. Yan, J. Yang, Z. Sun, C. Zhang, S. Li, and H. Yu, "Robust speed regulation for PMSM servo system with multiple sources of disturbances via an augmented disturbance observer," *IEEE/ASME Trans. Mechatronics*, vol. 23, no. 2, pp. 769–780, Apr. 2018.
[42] Z. Wu, H. T. Lyu, Y. L. Shi, and D. Shi, "On stability of open-loop operation without rotor information for Brushless DC motors," *Math. Problems Eng.*, vol. 2014, Jun. 2014, Art. no. 740498.
[43] J. Feng, Q. Wang, and K. Liu, "High-precision speed control based on multiple phase-shift resonant controllers for gimbal system in MSCMG," *Energies*, vol. 11, no. 1, p. 32, 2018, doi: 10.3390/en11010032.
[44] K.-T. Nam, H. Kim, S.-J. Lee, and T.-Y. Kuc, "Observer-based rejection of cogging torque disturbance for permanent magnet motors," *Appl. Sci.*, vol. 7, no. 9, p. 867, Aug. 2017.
[45] W. Qian, S. K. Panda, and J.-X. Xu, "Torque ripple minimization in PM synchronous motors using iterative learning control," *IEEE Trans. Power Electron.*, vol. 19, no. 2, pp. 272–279, Mar. 2004.
[46] D. E. Hill, "Dynamics and control of spacecraft using control moment gyros with friction compensation," *J. Guid., Control Dyn.*, vol. 39, no. 10, pp. 2406–2418, 2016.
[47] Q. Luo, D. Li, W. Zhou, J. Jiang, G. Yang, and X. Wei, "Dynamic modelling and observation of micro-vibrations generated by a single gimbal control moment gyro," *J. Sound Vib.*, vol. 332, no. 19, pp. 4496–4516, Sep. 2013.
[48] H. Bang, H.-S. Myung, and M.-J. Tahk, "Nonlinear momentum transfer control of spacecraft by feedback linearization," *J. Spacecraft Rockets*, vol. 39, no. 6, pp. 866–873, Nov./Dec. 2002.
[49] Z. Gao, "Scaling and bandwidth-parameterization based controller tuning," in *Proc. Amer. Control Conf.*, Denver, CO, USA, Jun. 2003, pp. 4989–4996.

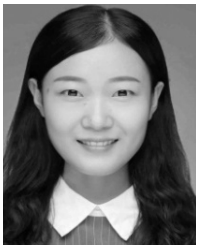

LIYA HUANG was born in 1991. She received the B.E. degree from the School of Automation and Electrical Engineering, University of Science and Technology Beijing, Beijing, China, in 2011. She is currently pursuing the Ph.D. degree with the School of Instrumentation Science and Optoelectronics Engineering, Beihang University, Beijing. Her main research is dynamics and attitude control of spacecraft.

ZHONG WU was born in 1970. He received the B.E. degree in automatic control from the North University of China, Taiyuan, China, in 1992, the M.E. degree in industrial automation from Tianjin University, Tianjin, China, in 1995, and the Ph.D. degree in control theory and control engineering from the Beijing Institute of Control Engineering, Beijing, China, in 1998. He is currently a Professor with the School of Instrumentation Science and Optoelectronics Engineering, Beihang University, Beijing. His research interests include dynamics and control of spacecraft, and drive and control of servo systems.

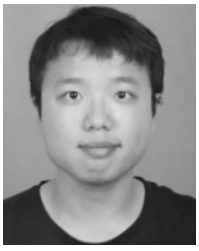

KAN WANG received the B.E. degree in detection guidance and control technology from Beihang University, Beijing, China, in 2010, where he is currently pursuing the Ph.D. degree with the School of Instrumentation Science and Optoelectronics Engineering. His research interests include measurement and control of servo systems.